

# Controlling Buoyancy-Driven Profiling Floats for Applications in Ocean Observation

Ryan N. Smith, *Member, IEEE*, and Van T. Huynh, *Student Member, IEEE*

**Abstract**—Establishing a persistent presence in the ocean with an autonomous underwater vehicle (AUV) capable of observing temporal variability of large-scale ocean processes requires a unique sensor platform. In this paper, we examine the utility of vehicles that can only control their depth in the water column for such extended deployments. We present a strategy that utilizes ocean model predictions to facilitate a basic level of autonomy and enables general control for these profiling floats. The proposed method is based on experimentally validated techniques for utilizing ocean current models to control autonomous gliders. With the appropriate vertical actuation, and utilizing spatio-temporal variations in water speed and direction, we show that general controllability results can be met. First, we apply an A\* planner to a local controllability map generated from predictions of ocean currents. This computes a path between start and goal waypoints that has the highest likelihood of successful execution. A computed depth plan is generated with a model-predictive controller (MPC), and selects the depths for the vehicle so that ambient currents guide it toward the goal. Mission constraints are included to simulate and motivate a practical data collection mission. Results are presented in simulation for a mission off the coast of Los Angeles, CA, USA, that show encouraging results in the ability of a drifting vehicle to reach a desired location.

**Index Terms**—Autonomous underwater vehicle (AUV), model-predictive control (MPC), ocean model, path planning, profiling float.

## I. INTRODUCTION

A profiling float is an underwater vehicle that is actuated only in the vertical (heave) direction, with the horizontal motion determined entirely by environmental parameters, e.g., ocean currents. The most famous example of a profiling float is the Argo float [1], as seen in Fig. 1. These vehicles were orig-

inally designed to map out deep-ocean currents, and are meant to be nearly Lagrangian in their motion.

The primary premise of this paper is to consider the interesting question: Can you control the horizontal motion of a profiling float? Investigating the control of mechanical systems is increasingly interesting when one considers systems that have unique methods of actuation and locomotion (e.g., biomimetic [2], energy harvesting [3], and variable buoyancy [4]) with specific constraints, or are underactuated (e.g., torpedo-shaped vehicles [5]) and subject to dynamic external forces (i.e., ocean currents). Thus, the profiling float provides a unique platform requiring a novel controller and planning methods, and posing many open questions and practical applications.

Specifically, the oceanographic community has a need for persistent observation platforms that remain *in situ* for months, and even years. Actively actuated (propeller-driven) vehicles are good for rapid data collections, but are limited in long-term endurance. Consequently, less actuated vehicles have emerged, facilitating energy savings and increased endurance. With reduced actuation, these vehicles have longer endurance, but are less able to achieve reliable trajectories, as their motion is dictated more by external forces (ocean currents) than by their own power (thrusters). To date, the primary region for the operation of these vehicles has been the deep ocean (>1000 m).

There is an increasing interest to operate profiling floats in highly dynamic coastal environments and confined regions, e.g., bays, to examine long-term variability, evolving features, and residence times. In such environments, these autonomous underwater vehicles (AUVs) would run aground or travel away from the desired sensing location if not controlled. Persistent monitoring in these near-shore and confined regions will help address the fundamental question of differentiating the processes that happen locally from those processes that happen remotely and are advected into the region.

A persistent presence is key to capturing the temporal variability of processes occurring over multiple scales (weeks to months, and possibly years). Currently, there are only a few types of AUVs that provide a high level of persistence: autonomous gliders [6], [7] and profiling floats [8], [9]. There has been considerable research done on the control of underwater gliders, e.g., [10]–[12]. We complement existing research by focusing on the control and planning for profiling floats, and examine applications of these vehicles for ocean science in dynamic environments.

## II. PREVIOUS WORK

A body of literature exists on path planning for actuated AUVs in the presence of currents, e.g., [13]–[15], and the

Manuscript received June 21, 2012; revised January 15, 2013 and April 15, 2013; accepted April 29, 2013. Date of publication August 06, 2013; date of current version July 10, 2014. This work was supported in part by the Early Career Academic Recruitment and Development (ECARD) Program of the Queensland University of Technology. The regional ocean model system (ROMS) predictions used were computed by the Jet Propulsion Laboratory (JPL), California Institute of Technology, Pasadena, CA, USA, under a contract with the National Aeronautics and Space Administration (NASA). This work was also supported by the Office of Naval Research Global under the Department of the Navy Grant N62909-11-1-4046. The U.S. Government has a royalty-free license throughout the world in all copyrightable material contained herein.

**Associate Editor:** R. Eustice.

R. N. Smith is with the Engineering and Physics Department, Fort Lewis College, Durango, CO 80301 USA (e-mail: rsmith@fortlewis.edu).

V. T. Huynh with the School of Electrical Engineering and Computer Science, Queensland University of Technology, Brisbane, Qld. 4001, Australia (e-mail: thanhvan.huynh@student.qut.edu.au).

Color versions of one or more of the figures in this paper are available online at <http://ieeexplore.ieee.org>.

Digital Object Identifier 10.1109/JOE.2013.2261895

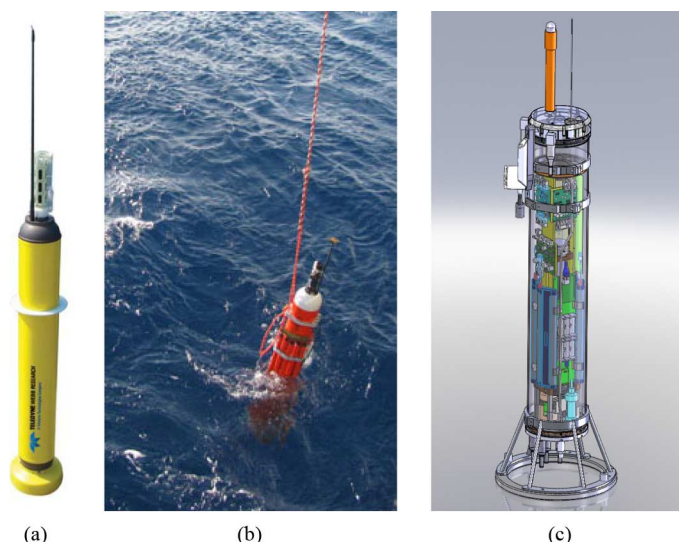


Fig. 1. Three examples of profiling floats that are currently in operation. (a) An Argo profiling float manufactured by Teledyne Webb Research, Inc. (Falmouth, MA, USA). (b) The Sounding Oceanographic Lagrangian Observer Thermal RECharging (SOLO-TREC) profiling float. Credit: The National Aeronautics and Space Administration (NASA)/Jet Propulsion Laboratory (JPL)/U.S. Navy/Scripps Institution of Oceanography. (c) The University of Rhode Island profiling float. Credit: Chris Roman, Graduate School of Oceanography, University of Rhode Island.

references contained therein. These studies primarily relate to quasi-steady-state ocean currents without consideration of vehicle actuation limits and often not identifying infeasible paths, particularly in strong ocean currents. Additionally, these intended applications assume that the AUV maintains a constant depth. The use of ocean currents to enable minimum-energy, continuous path planning in three spatial dimensions was proposed in [16]. Here the authors considered vehicle actuation limits using a multidimensional cost function for generating energy and time optimal paths in estuarine environments. Given the application domain, the current profile is assumed to be bidirectional and stratified. In an extension of this work, a new optimal (time and energy) path-planning approach was demonstrated with an actuated AUV in a tidally forced, dynamic bay [17]. This work illustrated the potential to use currents for improving vehicle range and endurance, as well as waypoint control in regions with tidally varying obstacles. Witt *et al.* [17] also exposed the utility of current variability with respect to depth in path planning for underwater vehicles.

Control of profiling floats is an emerging area of study with a very limited amount of prior investigation. Recent research has seen profiling floats applied in multiple applications from physical oceanography to underwater imaging, e.g., [9]. Such work has demonstrated an increased utility for the profiling float, and a need to investigate extending the control capabilities for such vehicles.

There has been analogous work published on the control of hot air balloons using wind prediction models [18]. In this work, the authors use a Markov decision process for probabilistic motion planning through arbitrary, uncertain vector fields, with an emphasis on high-level planning to solve a time-optimal problem. This work builds upon the well-understood problem of planning wind-efficient paths from the aeronautics com-

munity. In the AUV community, theoretical methods have been established for controlled Lagrangian particle tracking to analyze the offsets between physical positions of marine robots in the ocean and simulated positions of controlled particles in an ocean model [19]. This application considered autonomous gliders, which can apply controls to move horizontally, contrary to the profiling float.

The design of an ocean-scale, sensor web was proposed via intelligent control of deployed Argo floats in [20]. Dahl *et al.* examined the maximal coverage and motion toward a goal problems for multiple floating assets. The two algorithms presented in [20] were a constant depth strategy and a greedy approach to choosing a depth that used only a single time-step look-ahead in a large-scale ocean model with low spatio-temporal resolution. The model used has a 7-km horizontal resolution, with currents assumed to be constant over each day [21]. The application domain was the deep ocean, with discrete control actions occurring on the order of days. In a more dynamic environment, the development of a feedback controller for a single float operating in a tidally forced (single direction currents at each time step) region is presented in [22]. Jouffroy *et al.* take advantage of a near-zero current at depth and present a unique anchoring mechanism to enable loitering to avoid adverse currents when the tide is opposing the direction of desired motion. Thus, the proposed controller selects either the seafloor or the sea surface to enable waypoint tracking. The study in [22] was extended in [23], and provides a sufficient condition for controllability given three current directions that span the plane. The authors assume that the three currents can be taken as constant in both amplitude and direction. The work presented in [22] and [23], along with [24] and [25] is the first example of research into the development of control strategies for profiling floats to enable operation in dynamic and constrained coastal environments.

In this paper, we extend existing results to develop the tools that enable persistent monitoring with profiling floats in a dynamic coastal ocean environment. The five specific contributions of this paper are the following.

- 1) reformulation of the equations of motion for an AUV subjected to ocean currents;
- 2) controllability analysis for a profiling float in a dynamic, coastal environment;
- 3) derivation of a *controllability map* for probabilistic path planning with a deterministic ocean model;
- 4) a model-predictive controller (MPC) that computes the control actions (prescribed depth plan) to steer a profiling float between two given locations;
- 5) simulation results validating the proposed method for different current regimes within the region of interest.

The reformulation in contribution 1 is an extension of the initial presentation in [24]; this incorporates ocean model predictions into the equations of motion in the form of a control input, rather than a drift term or unknown component. The novelty is that, for the profiling float, we can directly change the effect of the ocean current, i.e., we can control it, by altering the depth of the vehicle. The controllability analysis of contribution 2 considers these reformulated equations of motion and provides necessary conditions for controllability of the reformulated dynamic system. The result provided is analogous to that presented

in [23] in that we show the necessity of a spanning set of velocity vectors for controllability. The difference in this paper is that we do not consider a minimal spanning set, but only require that the origin be within the convex hull of the chosen vectors. Additionally, we assume here that the currents are time varying in both direction and magnitude. With the necessary conditions for controllability, we present a *controllability map*, which was first introduced in [25]. This representation of the controllability of a region was specifically designed for mission planning of underactuated vehicles that exploit ocean currents. The map displays the current variability with respect to depth, providing a guide for planning purposes. Profiling floats will be more controllable in regions of more diverse currents, while an AUV with more actuation may prefer to go through regions of low variability to reduce uncertainty. Incorporating ocean model predictions in planning and control has been shown through field trials to be an effective method for reducing navigation error due to external disturbances for underactuated vehicles [26], [27]. A first version of the controller in contribution 4 was presented in [25], and is updated here with an examination of the stability and further validations provided in contribution 5.

The outline of the remainder of the paper is as follows. In Section III, we present a few examples of existing profiling floats to give a brief description of this unique vehicle. Section IV details the regional ocean modeling system; the predictive ocean model used in this study. In Section V, we present the standard equations of motion for the considered system, and then derive the reformulated equations based on the assumptions and information available. Given these new equations of motion, we then present an analysis of the controllability of this dynamic system, and provide the necessary conditions to achieve the general control that we desire. In Section VII, we utilize the ocean model and the necessary conditions to compute the controllability map, which provides a measure of expected controllability at each discrete location in the ocean model. We then apply an A\* planner, with the controllability map providing the underlying cost function, to compute a path connecting any two waypoints that has the highest expected controllability, and in turn, the greatest probability of successful execution. This path contains intermediate waypoints that steer the vehicle through highly controllable regions between the start and the goal. In Section VIII, we derive an MPC that steers the float along the computed path. The controller is designed to prescribe a depth for the float at each hour, so that the ocean currents push it along the path and eventually to the goal. We detail the constraints on the controller from a science-motivated point of view, and provide an examination of the stability and convergence of our proposed system. Section IX presents data from simulations in a coastal ocean region near Los Angeles, CA, USA. We conclude with some observations and present plans for future work and field deployments.

### III. PROFILING FLOATS

The vehicles considered here are commonly referred to in the literature as Lagrangian floats, profiling floats, or Lagrangian profilers; we use profiling floats. These vehicles have been utilized in ocean science research for multiple decades; see, e.g., [28]–[31]. We leverage recent advancements in ocean modeling and forecasting to examine the potential to increase

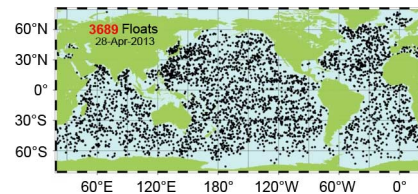


Fig. 2. Current location of Argo floats. Image courtesy of the Argo home page, <http://www.argo.ucsd.edu/index.html>.

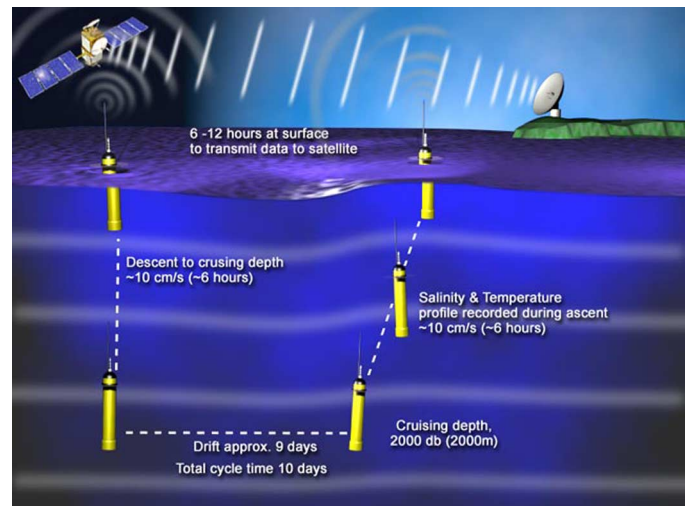


Fig. 3. Standard mission executed by Argo floats. Images courtesy of the Argo home page, <http://www.argo.ucsd.edu/index.html>.

the autonomy and utilization of this existing ocean science tool. The following sections present three existing examples of profiling floats, representing the range of operational capabilities.

#### A. Argo Float

Argo floats are widely used to gather data throughout our world's oceans in a cost-effective manner. These data are used in part to help us understand (and eventually predict) changes in both the atmosphere and ocean resulting from short- and long-term global climate change. Thousands of floats are deployed by ships of opportunity and sent off to gather data while drifting with the ocean's currents.

Currently, there are  $\sim 3700$  floats in operation (see Fig. 2, acquired on April 29, 2013), and more are being deployed all the time. At typically 10-day intervals, an Argo float surfaces over a 6-h interval while measuring temperature and salinity. Satellites determine its position once on the surface and the collected data are transmitted. The float then returns to its original density and sinks to drift until the cycle is repeated. Currently, deployed floats are designed to make about 150 such cycles, implying a deployment life of just over four years. For more information on Argo, see [1]. One standard operating mission scenario for Argo floats is shown in Fig. 3.

#### B. SOLO-TREC Float

SOLO-TREC is a float that is completely powered by renewable energy; the temperature differences in the ocean. SOLO-TREC draws upon the ocean's thermal energy as it alternately encounters warm surface water and colder conditions at depth. This thermal engine produces enough electricity

to operate the vehicle's science instruments, Global Positioning System (GPS) receiver, communications device, and buoyancy-control pump. SOLO-TREC has demonstrated the capability of continuously executing three to four dives per day [32].

### C. University of Rhode Island Float

The previous two profiling float examples provide a high-endurance platform, however, their operation is restricted to the deep ocean, i.e., > 1000-m depth. For coastal regions, these vehicles are not appropriate, which has promoted the development of a shallow-water profiling float.

The University of Rhode Island (URI, Kingston, RI, USA) has developed novel floats with an active ballasting system and acoustic altimeters, enabling them to position themselves anywhere in the water column, providing the ability to perform a range of drifting and profiling behaviors. These floats are able to operate successfully in areas of highly varied bathymetry, especially in near-shore environments. The float is built around a piston-style, volume-changing mechanism, allowing the buoyancy actuator to achieve profiling speeds of up to 20 m/min, with settling times  $O(10)$  s. For further information, see [9].

### D. Assumed Float Characteristics

We assume that the vertical position of the float within the water column can be accurately controlled, albeit limited, and the horizontal velocity is determined strictly by ocean currents; varying with depth and geographic location. We adopt a simple model for the profiling float, assuming that the vehicle motion is constrained to  $\mathbb{R}^3$ . Hence, we assume that the float is invariant in roll ( $\phi$ ), pitch ( $\theta$ ), and yaw ( $\psi$ ). We assume that the float is represented dynamically as a point mass and can change depth instantaneously.

## IV. OCEAN MODEL INPUT

The predictive tool that we utilize for general open ocean currents in the Pacific basin is the regional ocean model system (ROMS)—a split-explicit, free-surface, topography-following-coordinate oceanic model. ROMS is an open-source ocean model that is widely accepted and supported throughout the oceanographic and modeling communities. The model solves the primitive equations using the Boussinesq and hydrostatic approximations in vertical sigma (i.e., topography following) and horizontal orthogonal curvilinear coordinates. ROMS uses innovative algorithms for advection, mixing, pressure gradient, vertical-mode coupling, time stepping, and parallel efficiency. Detailed information on ROMS can be found in [33] and [34].

The ROMS output has three nested horizontal resolutions covering the U.S. west coastal ocean (15 km), the southern California coastal ocean (5 km), and the Southern California Bight (SCB; 2.2 km). The three nested ROMS domains are coupled online and run simultaneously exchanging boundary conditions, ultimately providing hourly hindcasts, nowcasts, and forecasts (up to 72 h) for southern California. The vertical resolution is nonuniform, providing data at 24 discrete depths ranging from 0 to 2000 m. Applications of this 4-D model implemented in

AUV path planning can be found in [35], [36], and the references contained therein.

## V. EQUATIONS OF MOTION

Given the assumptions of invariance in roll, pitch, and yaw, we define the three-degree-of-freedom configuration space of the float as  $Q = \mathbb{R}^3$ . We define a body-fixed coordinate frame  $B$ , located at the point  $(x_g, y_g, z_g)$ ; the center of gravity (CG) of the float. We assume that the vehicle can adjust to be neutrally buoyant at a prescribed depth, and the CG and the center of buoyancy (CB) are located along the same vertical axis in  $B$ . The state of the underwater vehicle is given by the vector  $\boldsymbol{\eta} \triangleq [b_1, b_2, b_3]^\top$  and describes the position of the float with respect to the inertial reference frame. The vertical position of the float ( $b_3(t)$ ) can be controlled, and the horizontal velocities ( $\dot{b}_1, \dot{b}_2$ ) are determined strictly by ocean currents. Let  $f, g, h : \mathbb{R}^3 \times \mathbb{R}^+ \mapsto \mathbb{R}$  represent the 4-D  $(x, y, z, t)$ ; three spatial plus time) north-south (zonal), east-west (meridional), and vertical currents, respectively. Velocity is taken to be positive eastward, northward, and opposing gravity. As the focus of this paper is to utilize the depth variation of the currents at each location, we suppress the horizontal dimensions for notational convenience. Specifically, given a latitude and longitude  $[(x, y)$  location], we define the ocean currents as functions of only depth ( $z$ ) and time ( $t$ ),  $f, g, h : \mathbb{R} \times \mathbb{R}^+ \mapsto \mathbb{R}$ . Then, conventionally, we would express the equations of motion in  $\mathbb{R}^3$  as

$$\dot{b}_1 = f(b_3, t), \quad \dot{b}_2 = g(b_3, t), \quad \dot{b}_3 = u_3(t) + h(b_3, t) \quad (1)$$

where  $u_3(t)$  represents the input control. In this scenario,  $u_3(t)$  corresponds to the chosen depth at a given time  $t$ .

Initially, we ignore vertical currents, i.e.,  $h(x, y, z, t) = 0$ , and thus,  $b_3(t) = u_3(t)$ . As ocean currents are not constant functions with respect to depth (Fig. 4), we can indirectly control the horizontal motion of the float by varying the depth of the vehicle. Hence, rather than considering the ocean currents as drift to the system, as is commonly done, we write them as a dependent input control; see [24] and [25] for a detailed treatment. Thus, for a given location, choosing a depth defines the direction of motion. This change in perspective of the ocean currents effectively reduces the problem to a planning problem in  $\mathbb{R}^2$  rather than in  $\mathbb{R}^3$ . The motion planning is then projected onto  $\mathbb{R}^2$ , with the depth ( $b_3$ ) acting as the input control ( $u_3$ ), which then defines the admissible velocities in the plane. Let  $H(z, t) = (f(z, t), g(z, t), 0)^\top$ , then we express the system as

$$(\dot{b}_1, \dot{b}_2, b_3)^\top = (0, 0, 1)^\top u_3(t) + H(b_3, t). \quad (2)$$

Note that we consider the state of the system to be defined by the velocities in the  $b_1$ - and  $b_2$ -directions and the position in the  $b_3$ -direction. We will define the control system as  $\Sigma = (Q, \mathcal{I}, U)$ , where  $Q = \mathbb{R}^2 \in \mathcal{C}^\infty$  is the configuration (state) space,  $\mathcal{I}$  is the set of input vector fields on  $Q$ , and the controls are given by  $U \subset \mathbb{R}^m$ , where  $m$  is the number of available choices for depth.<sup>1</sup> For this specific application, the configuration space is  $Q = \mathbb{R}^2$ , the input vector fields  $\mathcal{I}$  are the set of ocean current velocities at a particular location for the available depths, and the control  $U$  is the collection of available depths. Then,

<sup>1</sup>Given the ocean model presented in Section IV,  $m = 24$ .



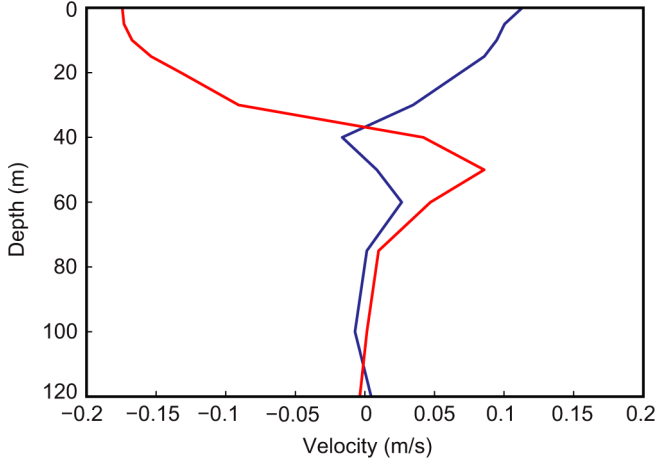


Fig. 4. An example vertical current profile prediction for a location off the coast of southern California. This is a ROMS prediction of ocean depth versus current velocity for the zonal (blue) and meridional (red) components located at 33.5° N, -118° E.

the motion planning problem is as follows: Given initial and final configurations  $\eta_0, \eta_f \in Q$ , respectively, find  $u \in U$  that steers the vehicle along a locally absolutely continuous curve  $\gamma : I \mapsto Q$ , where  $\gamma(0) = \eta_0$  and  $\gamma(T) = \eta_f$ . The only direct control input considered is the depth of the vehicle, i.e.,  $b_3(t) = u_3(t)$ . Since  $H(b_3, t)$  is a function of depth and time, we obtain indirect control on the vehicle velocity as we change the depth over time. For our analysis,  $H(b_3, t)$  is obtained from an ocean model, which is detailed in Section IV.

*Remark 1:* We remark that, although the state of the vehicle is  $\eta = [b_1, b_2, b_3]^\top$  (state in  $\mathbb{R}^3$ ), the states of interest are only  $\bar{\eta} = [b_1, b_2]^\top$  (state in  $\mathbb{R}^2$ ), corresponding to longitude and latitude, respectively. Since the depth is a control, we intrinsically maintain this state in this reduced control formulation. We will utilize  $\bar{\eta} = [b_1, b_2]^\top$  as the state for the remainder of the paper.

## VI. CONTROLLABILITY ANALYSIS

The approach to examining the controllability of the system presented here follows from Chow's theorem [37], and the extension of this result presented in [38]. These will be used to prove basic results for accessibility of the system, which will then provide a sufficient condition for the controllability of the system. A weak necessary condition for controllability is presented in [24], with a more strict condition provided in [23]. To begin, we reproduce the following three definitions from [39].

*Definition 6.1:* A controlled trajectory is a pair  $(\gamma, u)$ , where  $u : I \mapsto U$  is locally integrable and  $\gamma : I \mapsto Q$  is the corresponding locally absolutely continuous curve satisfying (2). We denote the set of controlled trajectories for  $\Sigma$  defined on  $[0, T]$  by  $C_{\text{traj}}(\Sigma, T)$ .

*Definition 6.2:* For  $x_0$  in  $Q$ , the set of states that are reachable in time exactly  $T$  is denoted by  $\mathcal{R}_{\Sigma}(x_0, T) = \{\gamma(t) \mid (\gamma, u) \in C_{\text{traj}}(\Sigma, T), \gamma(0) = x_0\}$ . Also, the set of states that are reachable in time at most  $T$  is given by  $\mathcal{R}_{\Sigma}(x_0, \leq T) = \cup_{t \in [0, T]} \mathcal{R}_{\Sigma}(x_0, t)$ .

*Definition 6.3 (Notions of Controllability):* Let  $\Sigma = (Q, \mathcal{I}, U)$  be a  $C^\infty$ -control-affine system and let  $x_0 \in Q$ .

- 1)  $\Sigma$  is accessible from  $x_0$  if there exists  $T > 0$  such that the interior of  $(\mathcal{R}_{\Sigma}(x_0, \leq t)) \neq \emptyset$  for  $t \in ]0, T]$ .

- 2)  $\Sigma$  is controllable from  $x_0$  if, for each  $x \in Q$ , there exists  $T > 0$  and  $(\gamma, u) \in C_{\text{traj}}(\Sigma, T)$  such that  $\gamma(0) = x_0$  and  $\gamma(T) = x$ .
- 3)  $\Sigma$  is small-time locally controllable (STLC) from  $x_0$  if there exists  $T > 0$  such that  $x_0$  is in the interior of  $(\mathcal{R}_{\Sigma}(x_0, \leq t))$  for each  $t \in ]0, T]$ .

Since the revised equations in (2) present a driftless system, we can invoke a local version of Chow's theorem to infer the controllability. In particular, we state the following corollary to the more general result of [40].

*Corollary 1 (Controllability of Driftless Systems):* Let  $\mathcal{F} = \{f_0, f_1, \dots, f_m\}$  be  $C^\infty$ -vector fields on  $Q$  with  $f_0$  identically zero. The pair  $(Q, \mathcal{F})$  is properly STLC from  $x_0$  if  $\text{Lie}^\infty(\mathcal{F})_{x_0} = T_{x_0}Q$ . Here,  $\text{Lie}^l(\mathcal{D})$  is the distribution generated by Lie brackets of degree  $l$  in vector fields taking values in  $\mathcal{D}$ . For  $l = \infty$ ,  $\text{Lie}^l(\mathcal{D})$  represents the involutive closure of  $\mathcal{D}$ . From this result, the choice to write the drift vector field as a controlled input vector field should be evident.

### A. Conditions for Controllability

We are interested in verifying controllability for (2) in  $\mathbb{R}^2$ . This can be accomplished by examining the accessibility set; the set of all admissible motions from each configuration.

*Lemma 1:* Given  $\eta$ , the accessibility set for the system in (2) is given by  $\mathcal{A} = \text{Lie}^\infty(\mathcal{I})$  for  $\mathcal{I} = \{(0, 0, 1)^\top, H(z, t)^\top\}$ .

The controllability of  $\mathcal{A}$  is assessed by the use of the following proposition.

*Proposition 1:* The system given in (2) is controllable in  $\mathbb{R}^2$  if and only if the convex hull of the accessibility set  $\mathcal{A}$  is compact and contains the origin.

The proof of Proposition 1 is a standard result from control theory, and in the interest of space, we omit the details here. We refer the interested reader to [39] for a proof of this result.

Proposition 1 presents an analytic analysis of the control of a profiling float that can move vertically through the water column. At first glance, the ocean may appear too dynamic and complex to incorporate into such an analytic formality. However, here, we utilize general trends and an ocean model to assist in planning and control techniques, since we are not interested in precise trajectory tracking but a more general notion of control. It is also of interest to note that, although the accessibility set  $\mathcal{A}$  may contain several vector fields to define the convex hull, it is sufficient for controllability of the system to have only three vectors that span the plane; see [23] for details.

## VII. PATH PLANNING

Here, we present the path-planning method utilized in this research to steer the float between start and goal locations. Note that for persistent monitoring applications in the ocean, it is not imperative that a vehicle exactly follow a prescribed path, or precisely achieve the goal location. In this environment, the tolerances are measured in hundreds of meters, as opposed to centimeters for similar applications in aerial and terrestrial robotics. It is most important that the vehicle have a persistent presence and remain within the desired region of interest.

Determining a traversable path for a profiling float requires examining the controllability of the region of operation. With

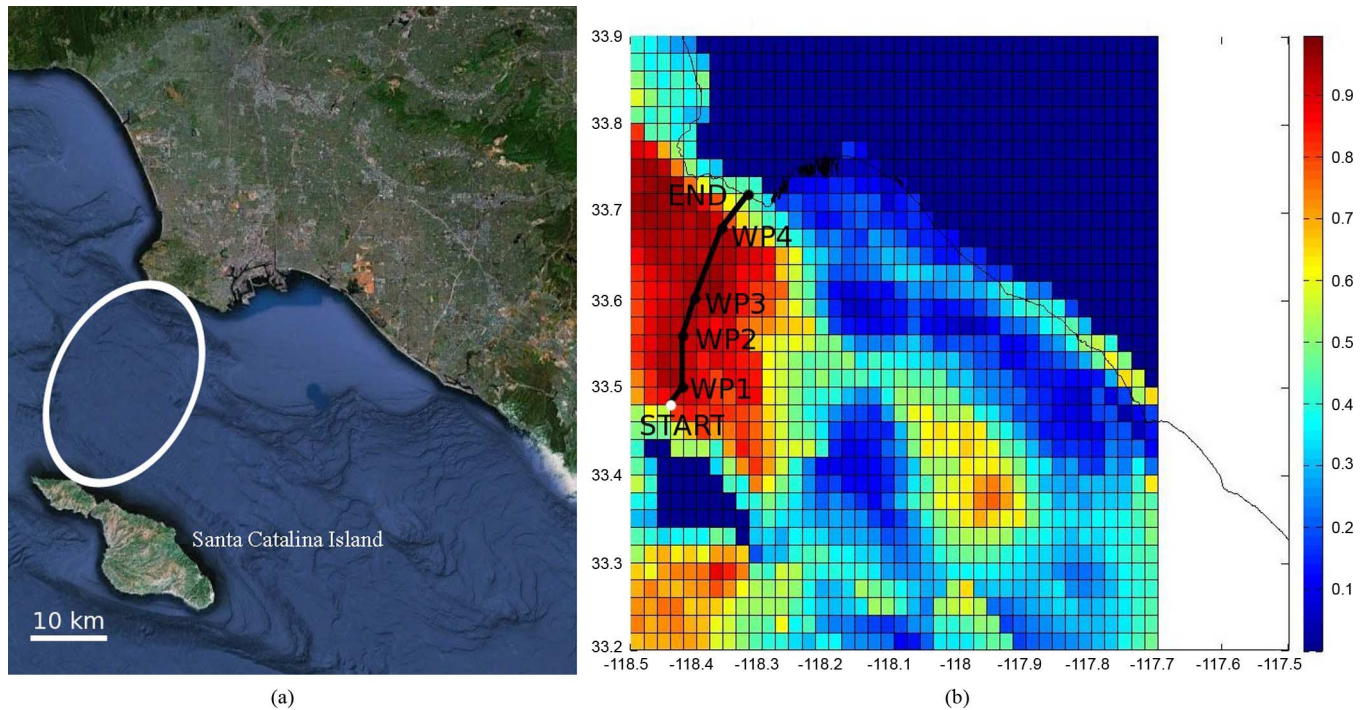


Fig. 5. (a) The geographic area of interest highlighted by the white oval. (b) The controllability heat map computed for this geographic region. Note that the two images are not the same scale. (a) Google Earth image of the geographic region of interest; the San Pedro Bay off the coast of southern California. (b) The controllability heat map generated from ocean model predictions with the optimal  $A^*$  path overlaid in black. Blue refers to areas of low controllability, and red are areas of high controllability.

this information, a path can be computed that provides sufficient controllability to reach the goal location. The outcome of this path planning is the computation of intermediate waypoints between the start and goal locations that guide the vehicles through the greatest diversity of currents, and thus the highest probability of reaching the goal location. To examine the controllability within a region, we construct a controllability map from the ROMS predictions [25]. This map presents the diversity and general trends of the ocean currents as a probabilistic scalar field, upon which we plan a path with the greatest likelihood of success.

#### A. The Controllability Map

The key integration of the ocean model in this research is the ability to predict areas that provide a high level of local controllability for the float, i.e., areas that satisfy Proposition 1. The result of this analysis is a controllability map upon which we can plan. For each hour of available data, we project the velocity vector of each depth bin into a single plane at each discrete node in the model output. In the plane, we compute the convex hull of the set of velocity vectors at each location. For each location and each time step, we produce a binary output; 1 if the convex hull of the velocity vectors contains the origin (model node), and 0 if it does not. Then, we sum these outputs over all hours and compute the percentage that each location provides a controllable scenario, i.e., satisfies Proposition 1. A resultant heat map of controllability, for the geographic region of interest (Fig. 5), is presented in Fig. 5 with blue referring to areas of a low percentage of controllability, and red the areas with a high percentage of controllability. More specifically, the red regions are locations that are expected to provide a sufficient

variability in the ocean current, with respect to depth, over the proposed time period to allow for local controllability. The blue regions are areas that will likely exhibit a more constant current direction with respect to depth, for the given time duration.

*Remark 2:* Note that since the controllability map is intended to be computed from historical data before a mission, we are not interested in utilizing it to compute the optimal path for the entire duration of deployment. Rather, we are simply computing a path *a priori* that has the greatest likelihood of success, given the prior information that we have at hand. This view of the model data provides general trends that can be exploited through the proposed method. We constrain the float to surface at least every 70 h to update the model predictions so that the proposed controller uses the most recent predictions as they become available. For shorter duration mission planning, e.g., using a single ROMS prediction for computing optimal AUV controls for a mission lasting  $< 70$  h, the proposed controllability map technique is not optimal. Rolling all the data of the 4-D model into a single scalar field loses a lot of information in this scenario. For example, full controllability at a location is not necessary if you have currents in the intended direction of travel at that location. We refer the interested reader to previous publications by the authors [35], [36] for alternate applications of ocean models in these shorter or iterative mission planning tasks for AUVs.

#### B. Determining the Path

Given the controllability map described in Section VII-A, we can implement a path planner based on the desired level of predicted controllability. Given the graph structure of the ocean model output, and the straightforward cost function, we implement a simple  $A^*$  planner to compute a path from the start

location to the goal. This produces intermediate waypoints at discrete locations that correspond with the nodes in the ocean model output. The optimization constraint considered is to minimize the cost function  $c(p) = 1 - p$  over the path between the start and the goal, where  $p$  is the percentage of controllability at a given node. The path computed by the A\* planner will, in general, be different than the straight line path connecting the start and goal waypoints since it guides the float through areas of maximal controllability.

A path planned by this method is given by the black line in Fig. 5 on an example controllability map. The start location is just off the tip of Catalina Island, CA, USA, and is labeled START and is depicted by a white dot in Fig. 5. The end of the path is labeled END, and is given by the black dot and is located just off the California coast. The four dots (WP1, WP2, WP3, and WP4) along the path are intermediate waypoints computed by the A\* planner.

*Remark 3:* For practical reasons, we cannot assume to know or have a prediction of the ocean currents *a priori* for the entire duration of a long-term deployment (weeks to months). The ROMS used here only provides a 72-h forecast, which is insufficient for preplanning even a week-long mission. To circumvent this, we rely on regional trends in the structure of ocean currents within a specific area of interest. Specifically, in the chosen area of interest, there are three distinct seasons when considering ocean dynamics: an upwelling season from March through May and partially into June, the summer/early fall season runs from mid-June into October, and the transition season that occurs from November through February. During each season, we can assume a similar current structure to persist. For example, from June to October, the average flow tends to be downcoast (southerly), while from November to March, the average flow tends to be upcoast (northward) [41], [42]. To this end, the proposed planning methodology is designed to generate the controllability map based on a set of historical model predictions (approximately two weeks for the presented simulations), plan a path for the highest likelihood of success on this map, then execute this path based upon model updates as they become available in real time. Hence, although the presented results are simulations, they were conducted as if the float were operating in the ocean. In Section VIII, we provide constraints on the controller to adequately account for need to update current predictions as they become available.

## VIII. CONTROL STRATEGY

The chosen mission is to persistently execute a transect crossing the channel between the U.S. west coast and Catalina Island, as highlighted in Fig. 5. The mission is scientifically motivated by a desire to understand the nutrient flux within the San Pedro Bay. Given this science motivation and the ROMS output, we impose the following operational constraints upon our controller.

- ROMS provides 72-h predictions each day, thus we fix a maximum of 70 h between surfacings.
- For safety, we neither want to surface frequently nor stay on the surface for extended periods of time. Thus, we set a minimum 6-h limit between surfacings, and only allow the float to remain on the surface for 1 h.

- Motivated by the underlying science, we require the float to perform periodic, full-depth, vertical profiles. This is implemented by requiring the float to go to the seafloor (or maximum prescribed depth) for the time-step immediately preceding a scheduled surfacing.
- We do not constrain the float to follow a prescribed trajectory, but provide control such that each waypoint is achieved to within a user-defined tolerance ( $r$ ).

We base the controller design on the equations of motion derived previously. In Sections V and VI, we present an analytic representation for the system and the controllability. Given that the ROMS output is discrete in time, the input to the controller will not change over a single time epoch (for ROMS, this is 1 h), and hence, a computed control action would remain constant over that time period. Additionally, energy consumption on this type of vehicle directly corresponds to changes in buoyancy (depth), and reducing these changes increases the deployment time, giving a more persistent presence. Thus, we are motivated to consider a discrete-time controller for this application.

To convert from the continuous equations to the discrete-time application, we define the following variables. Let the state of the system be defined by  $\bar{\eta} = [b_1, b_2]^T \in \mathbb{R}^2$ , and the system output be defined by  $\bar{\nu} \in \mathbb{R}^2$ . Since the ROMS output contains 24 discrete depths,  $\mathcal{I} = \{\mathbf{u}_1, \dots, \mathbf{u}_{24}\}$  is the set of input control vectors, where  $\mathbf{u}_j = [0, \dots, 0, 1, 0, \dots, 0]^T$  with the nonzero entry as the  $j$ th component of the vector. Hence, the control input is bang–bang, and we interpret that a control of  $\mathbf{u}_1$  commands the float to the sea surface, while a control of  $\mathbf{u}_j$  for  $j \in \{2, \dots, 24\}$  commands the float to the associated depth within the ROMS output discretization. Function  $u_3(t)$  in (1) is then a piecewise constant function of the assigned depths for the float, and we let  $\mathbf{u}$  represent the discrete-time control input to the system. Since the ocean is not always 2000 m deep (maximum ROMS depth,  $j = 24$ ) in the operational region, or in the event that we would like to limit the operational depth of the vehicle within the controller, we allow  $\mathbf{u}_j = [0, \dots, 0]^T$  for  $j > M$ , where  $M$  is the maximum ocean depth allowed for a given location. For the examples presented here, we set a maximum depth of 1000 m, corresponding to  $M = 21$ , although the actual depth at a location may be less than this in many instances.

We choose to implement a robust constrained finite horizon model-predictive controller (RCFMPC). We assume that there are no sudden changes in the velocity of the ocean currents with respect to time. Given the system parameters defined above, we write a discrete-time, linear time-varying (LTV) system as follows:

$$\bar{\eta}(k+1) = \mathbf{I}_2(k)\bar{\eta}(k) + \mathbf{B}_{\bar{\eta}}(k)\mathbf{u}(k) \quad (3)$$

$$\bar{\nu}(k) = \mathbf{C}(k)\bar{\eta}(k). \quad (4)$$

Here,  $\mathbf{I}_2$  is the  $2 \times 2$  identity matrix. Matrix  $\mathbf{B}_{\bar{\eta}}(k)$  is a  $2 \times 24$  matrix giving the  $x$  and  $y$  velocities at each depth at location  $\bar{\eta}$  from the ROMS model. This matrix is obtained by interpolating a set  $\mathbb{B}$  consisting of four similar matrices output from ROMS; one matrix for each discrete ROMS grid point that defines the bounding box around the current location of the float. The set  $\mathbb{B}$  acts as a lookup table for the predicted currents at a given spatio-temporal location, and is taken from the 7826 total, discrete nodes in the ROMS output. Matrix  $\mathbf{C} = \mathbf{I}_2$ .

Let  $k$  refer to the current time step,  $i = 1, \dots, m$  define the finite control horizon, and  $n = 1, \dots, N$  define the finite prediction horizon. Let  $\mathbf{u}(k+i|k)$  be the control action at time  $k+i$ , given we are at time  $k$ . We assume that there is no control action after time  $k+m$ , i.e.,  $u(k+i|k) = 0$ ,  $i \geq m$ . From the model in (3), the RCFMPC has the following objective:

$$\min_{\substack{\mathbf{u}(k+i|k), \\ i=0,1,\dots,m}} \max_{\mathbf{B}_{\bar{\eta}}(k) \in \mathcal{B}} J_n(k) \quad (5)$$

where

$$J_n(k) = \sum_{i=0}^n (\bar{\eta}(k+i|k)^T \mathbf{Q}_1 \bar{\eta}(k+i|k) + \mathbf{u}(k+i|k)^T \mathbf{R} \mathbf{u}(k+i|k)). \quad (6)$$

Here,  $\mathbf{Q}_1 > 0$  and  $\mathbf{R} > 0$  are symmetric, positive-definite, weighting matrices, and  $n$  is the finite horizon, or number of look-ahead steps. From (3) and (6), note that  $J_n(k)$  is a function of both  $\mathbf{B}_{\bar{\eta}}(k)$  and  $\mathbf{u}(k)$ , although we suppress this notation here. Set  $\mathcal{B}$  is the set of possible matrices for  $\mathbf{B}_{\bar{\eta}}(k)$ . Since we compute  $\mathbf{B}_{\bar{\eta}}(k)$  as an interpolation of the ROMS output, there is an inherent uncertainty in this computation. We allow  $\mathcal{B}$  to have finitely many values to incorporate this uncertainty into the controller.

Since  $\mathbf{Q}_1$  and  $\mathbf{R}$  are positive definite, (5) is equivalent to minimizing the objective (distance between the current state and the goal) at each step of the prediction horizon  $n = 1, \dots, N$ , with the largest (worst case) value of  $J_n(k)$ , as shown in

$$\min_{\substack{\mathbf{u}(k+i|k), \\ i=0,1,\dots,m}} \max_{\mathbf{B}_{\bar{\eta}}(0) \in \mathcal{B}} J_0(k) \max_{\mathbf{B}_{\bar{\eta}}(1) \in \mathcal{B}} J_1(k) \dots \max_{\mathbf{B}_{\bar{\eta}}(N) \in \mathcal{B}} J_N(k). \quad (7)$$

The desired RCFMPC is subject to the following constraints.

- Output

$$\bar{\mathbf{v}}(k) \rightarrow 0, \quad \text{for } k \rightarrow \infty. \quad (8)$$

Since the destination waypoint is chosen to be the origin, we always have the final state approaching zero.

- Input

$$\mathbf{u}(k) \in \mathcal{I}. \quad (9)$$

- Acceptable current directions: Let  $\boldsymbol{\tau}_1(k) = \bar{\eta}(k+1) - \bar{\eta}(k)$ ,  $\boldsymbol{\tau}_2(k) = -\bar{\eta}(k)$ , and  $\beta$  be an angle about the azimuth from the current location of the vehicle to the prescribed waypoint that defines a range for acceptable ocean currents to choose. This gives the following constraint:

$$\boldsymbol{\tau}_1^T(k) \boldsymbol{\tau}_2(k) \geq \cos \beta \|\boldsymbol{\tau}_1(k)\| \|\boldsymbol{\tau}_2(k)\|. \quad (10)$$

- Terminal

$$\bar{\mathbf{v}}(N) \in \mathcal{B}_r \quad (11)$$

where  $\mathcal{B}_r$  is a ball of radius  $r$  that is a user-defined parameter for the control algorithm.

We impose the angle of acceptable current constraint in (10) to ensure that the velocity vector at a chosen depth generally points toward the destination waypoint. This constraint reduces the number of depth choices to only those that provide a current that reduces the distance to the goal at each time step. The

implementation of this constraint was motivated by [22], where the guiding angle constraint is defined as a symmetric sector of sight about the line of sight between the actual position of the vehicle and the destination point. It is worth noting that the guiding angle constraint in (10) is not necessary, but imposed to speed up the convergence of the RCFMPC. Eliminating or relaxing this constraint could result in a movement that increases the distance to the goal for a given time step. This scenario is much more flexible for execution, but requires onboard recomputation of the path at each stage to ensure that the vehicle does not diverge into a region where it cannot escape.

*Remark 4:* Observing the objective equation (5) with constraint equations (8)–(11), we remark that the RCFMPC is a hybrid, nonlinear problem. There is no direct method to solve this problem explicitly. In our approach, we take advantage of the constraint equation (9), noting that  $\mathcal{I}$  is a finite set with deterministic values. As a result, the RCFMPC is feasible by only allowing a finite set of values for the control input. Additionally, we utilize the fact that near-zero currents exist at depth (near the seafloor) and possibly other depths within the water column. The vehicle can thus prescribe a depth with little to no current, implying minimal deviation from its path, to wait for more favorable currents to become available in the future. This takes advantage of the dynamic nature of the spatio-temporal variability of ocean currents, and that the path was planned by the use of the controllability map to be through an area of high current diversity, to provide a solution to the control problem.

#### A. Stability and Convergence

Having defined the RCFMPC for a profiling float, we now examine the stability of this system in the context of the application. Given that  $\mathbf{B}_{\bar{\eta}}(k)$  represents a discrete and deterministic prediction of the ocean currents, and the chosen control  $\mathbf{u}(k)$  is bang-bang, we cannot expect to provide strict guarantees on the rate or accuracy of convergence of the proposed controller. However, the considered vehicle does not require such guarantees and precise control for operation, but rather a broad notion of movement in a given direction or toward a chosen location. By using the controllability map presented in Section VII-A, we can compute a path connecting any two locations that has the highest probability of finding a control (ocean current) in the prescribed direction at each time epoch (each hour). Additionally, as the proposed application is intended to maintain a persistent presence in the ocean, the time constraint is the deployment life of the vehicle. Hence, in the context of the proposed application, we are interested in asymptotic convergence ( $t \rightarrow \infty$ ) to a region ( $\mathcal{B}_r$ ). Since the authors work closely with the developers of the ocean model utilized here, one intent of this research is to develop a continuous feedback between the vehicle and the ocean model during field trials. As the motion of the vehicle is purely based on currents, assimilating the deployment data will increase the accuracy of future predictions, and in turn, improve the rate and accuracy of convergence of the RCFMPC.

To demonstrate the convergence and stability of the proposed controller, we first assume that the control horizon equals the prediction horizon, i.e.,  $m = N$ . It will always be the case for our RCFMPC that  $m \leq M$ , and for strict inequality, we reduce to the assumed scenario by setting the control actions to zero for



times exceeding the control horizon. Let  $\zeta = \bar{\boldsymbol{\eta}}(k+i|k)$ , and define the value function  $V_k : \mathbb{R}^2 \mapsto \mathbb{R}$  as

$$V_k(\zeta) = \min_{\mathbf{u}(k+i), \dots, \mathbf{u}(k+m-1)} \times \sum_{\tau=k+i}^{k+m-1} (\bar{\boldsymbol{\eta}}(\tau|k)^\top \mathbf{Q}_1 \bar{\boldsymbol{\eta}}(\tau|k) + \mathbf{u}(\tau|k)^\top \mathbf{R} \mathbf{u}(\tau|k)) \quad (12)$$

subject to  $\bar{\boldsymbol{\eta}}(k+i+1|k) = \mathbf{I}_2 \bar{\boldsymbol{\eta}}(k+i|k) + \mathbf{B} \bar{\boldsymbol{\eta}}(k+i|k) \mathbf{u}(k+i|k)$ . Then, (12) is the minimum cost-to-go for the MPC starting at state  $\zeta$  at time  $t = k+i$ . We note that the final cost for the last step is simply the predicted final state cost, given by  $V_m(\zeta) = \zeta^\top \mathbf{Q}_1 \zeta = \bar{\boldsymbol{\eta}}(m|m)^\top \mathbf{Q}_1 \bar{\boldsymbol{\eta}}(m|m)$ . Now, if we have  $V_{k+1}(\zeta)$ , then it has a Lyapunov function form at time  $t = (k+i+1)$  given by

$$V_{k+1}(\zeta) = \zeta^\top \mathbf{P}_{i+1} \zeta \quad (13)$$

with  $\mathbf{P}_{i+1} = \mathbf{P}_{i+1}^\top \geq 0$ . This is supported by the fact that the final state cost is  $V_m(\zeta) = \zeta^\top \mathbf{Q}_1 \zeta$ , and at time  $t = k+m$ ,  $\mathbf{P}_m = \mathbf{Q}_1$ . Considering this cost minimization as a dynamic program, we can write

$$V_k(\zeta) = \min_w [\zeta^\top \mathbf{Q}_1 \zeta + w^\top \mathbf{R} w + V_{k+1}(\mathbf{I}_2 \zeta + \mathbf{B} w)] \quad (14)$$

where  $\mathbf{B} = \mathbf{B} \bar{\boldsymbol{\eta}}(k+i|k)$ ,  $\zeta^\top \mathbf{Q}_1 \zeta + w^\top \mathbf{R} w$  is the cost incurred at  $t = (k+i)$  if  $\mathbf{u}(k+i|k) = w$ , and  $V_{k+1}(\mathbf{I}_2 \zeta + \mathbf{B} w)$  is the minimum cost-to-go from where the float ends up at  $t = (k+i+1)$ . This then gives  $V_k$  recursively in terms of  $V_{k+1}$  as the Hamilton–Jacobi equation in (15), with any minimizing  $w$  giving the optimal  $\mathbf{u}(k+i|k)$  as the argument of the minimum of  $w^\top \mathbf{R} w + V_{k+1}(\mathbf{I}_2 \zeta + \mathbf{B} w)$

$$V_k(\zeta) = \zeta^\top \mathbf{Q}_1 \zeta + \min_w [w^\top \mathbf{R} w + V_{k+1}(\mathbf{I}_2 \zeta + \mathbf{B} w)]. \quad (15)$$

Solving for  $\mathbf{u}(k+i|k)$  is straightforward when  $w$  is a continuous variable, with a result similar to that of a linear quadratic regulator (LQR). However,  $w$  here is bang–bang, and we cannot solve for the closed-form control, as in the case of the LQR.

Since  $w$  is bang, we can write

$$w^* = \mathbf{F} \zeta + \epsilon \quad (16)$$

$$\mathbf{B} w^* = \mathbf{B} \mathbf{F} \zeta + \mathbf{B} \epsilon \quad (17)$$

where  $\mathbf{F} = -(\mathbf{R} + \mathbf{B}^\top \mathbf{P}_{i+1} \mathbf{B})^{-1} \mathbf{B}^\top \mathbf{P}_{i+1} \mathbf{I}_2$  and  $|\epsilon| < 1$ . We remark that since we allow the float to choose a depth of near-zero currents in the event of no other favorable option, (16) will always be satisfied for the choice of  $\epsilon$ . Additionally, the size of  $\epsilon$  depends on the angle constraint  $\beta$ ; as  $\beta \rightarrow 180^\circ$  (allowing any direction of current), we have that  $\epsilon \rightarrow 0$ .

Stability of the system is demonstrated by solving the inequality  $V_{k+1}(\zeta) \leq V_k(\zeta)$ ; the state of the system is approaching the origin. This leads to the following linear matrix inequality (LMI):

$$\begin{bmatrix} \mathbf{Q}_1 & \mathbf{B}^\top & 0 \\ \mathbf{B} & \mathbf{R} + \mathbf{B}^\top \mathbf{P}_{i+1} \mathbf{B} & 0 \\ 0 & 0 & \mathbf{R} + \mathbf{B}^\top \mathbf{B} \end{bmatrix} \geq 0. \quad (18)$$

Given (18), then we have  $\zeta^\top \mathbf{P}_{i+1} \zeta - \zeta^\top \mathbf{P}_i \zeta \leq \epsilon^\top (\mathbf{R} + \mathbf{B}^\top \mathbf{B}) \epsilon$ , where  $(\mathbf{R} + \mathbf{B}^\top \mathbf{B})$  is positive definite and  $\epsilon$  is a small positive constant. Thus, the state  $\zeta = \boldsymbol{\eta}(k+i|k)$  will converge to a region of radius  $r$ , with the size of  $r$  based on the magnitude of the eigenvalues of  $[\mathbf{R} + \mathbf{B}^\top \mathbf{B}]$ . Thus, we have that the system is stable and will converge asymptotically to a region under the given constraints.

*Remark 5:* If the interpolation of ROMS is exact, then  $\mathbf{B} = \mathbf{B} \bar{\boldsymbol{\eta}}(k)$  is unique, and we need only solve the single LMI, as presented in (18). However, there is an associated uncertainty with the interpolation that should be considered for practical implementation. To handle this, we compute the maximum uncertainty from the interpolation method. Note that here we do not attempt to estimate the uncertainty of ROMS, only the interpolation. Then, we have a bounding rectangle of uncertainty about each interpolated point. We project this uncertainty into the LMI in (18) by assuming that, at each time step,  $\mathbf{B}$  has four discrete values (the corners of the bounding rectangle) and we solve (18) four times to find the control that drives the system toward the desired waypoint. This makes the proposed controller robustly constrained, even in the presence of uncertainty. Further incorporating the uncertainty of ROMS into this framework will require extensive field trials to ground-truth predictions, and is the scope of future work for this project.

### B. Solving the Control Problem

Now that we have verified convergence, we present the methodology for solving the problem. Solving the RCFMPC is equivalent to solving a multiparametric mixed integer nonlinear programming (mp-MINLP) problem. There are not many robust techniques applicable to solving the general mp-MINLP problems. Available tools, e.g., the MPT and Yalmip toolboxes [43], [44], handle special cases of mp-MINLP. However, finding an effective algorithm to solve the general mp-MINLP is still an open problem. Also, the aforementioned tools require significant computation effort when dealing with problems of high dimension.

Two primary approaches have been proposed to solve the multiparametric, mixed-integer problems. A first approach is based on branch and bound methods [45], where a multiparametric linear problem (mp-LP) is solved at each node of the branch and bound tree. Here, a lower bound for the optimization is given by the solution at the root node, and the upper bound is provided by the solution at a node where all the integer variables have been fixed. An alternative approach is to solve mp-LPs when the integer variables are fixed at the optimal value, as determined by a mixed integer linear program (MILP) [46], rather than solving mp-LP problems with integer variables relaxed in the interval  $[0, 1]$ . Both of these methods require significant computation effort, as the search tree expands nonlinearly with respect to the dimension of the state variables. Motivated by [47], we initially implemented an algorithm based on greedy, depth-first search [25]. Algorithm 1 is an extension to our previous work that includes the full vertical profile constraint mentioned at the beginning of Section VIII. The details of incorporating a feedback loop for our controller are given in Section VIII-C.

---

**Algorithm 1:** Solver for the RCFMPC, including occasional full vertical profiles.
 

---

**Input:** Operation time, minimum surfacing times (SURF), an initial waypoint  $\mathbf{W}_{init} = \{X_a, Y_a\}$ , a target waypoint  $\mathbf{W}_{final} = \{X_b, Y_b\}$ , predicted ROMS data, and prediction horizon  $m$ .

**Output:** The switching sequence of depth control inputs.

```

/* Initialize variables                                     */
1  $i \leftarrow 0$ 
2  $\mathbf{Y}(k+i|k) \leftarrow$  Current Position
3 for  $i \leftarrow 0$  to  $m$  do
    /* If the profiler is within the prescribed radius, then STOP */
4     if  $\|\text{Position}(k+i|k)\| \leq r_B$  then
5         return Depth, Position
6     /* Else, proceed to solve for m time horizons ahead */
7      $\mathbf{B}(k+i|k) \leftarrow$  InterpolateB( $\mathbf{Y}(k+i|k)$ )
    /* Infer matrices B at vertices of the uncertainty polytopes */
8     InferVertexB(Uncertainty Polytopes)
9     if  $i == m - 1$  then
10        SeabedCurrents( $m - 1$ )
11        SurfaceCurrents  $\leftarrow$  SurfaceCurrents( $m$ )
12    if Operation time  $\geq$  SURF and CheckConstraints(SurfaceCurrents) then
13        Depth( $m - 1$ )  $\leftarrow$  Sea bed
14        SurfFlag  $\leftarrow$  1
15    else if SurfFlag == 1 then
16        Depth( $m$ )  $\leftarrow$  Sea surface
17        SurfFlag  $\leftarrow$  0
18    else
19        for  $j \leftarrow 0$  to  $(n_u + 1)$  do
20            iPositions  $\leftarrow$  InferNextPosition()
21            pPositions  $\leftarrow$  CheckConstraintsOfMPC(iPositions)
22            Objectives  $\leftarrow$  MaxObjOfMPC(pPositions)
23            [Depth( $k+i|k$ ), Position( $k+i|k$ )]  $\leftarrow$  MinObj(Objectives)
24 return Depth, Position

```

---

### C. A Closed-Loop Solution

Given the reduced controllability of the profiling float and the nature of ocean currents, it is foreseeable that the vehicle will diverge from the prescribed path, even with the proposed RCFMPC. Potential scenarios for such an occurrence may include a poor prediction by ROMS, or a significant time navigating without a ROMS update. We propose a feedback loop for the RCFMPC, as depicted in Fig. 6.

In the proposed design, the number of surfacings (SURF) is an input to the RCFMPC. We would like the surfacing interval to be adaptive throughout the mission, but constrained within given limits. Hence, we incorporate SURF into a feedback loop by inserting a check on the difference in actual position versus estimated position (DIFFERENCE) within the overall control system. Here, DIFFERENCE is computed using the actual lo-

cation if the float is on the surface, or an estimated location while the vehicle is underwater. This feedback adjusts SURF throughout the mission with the following two simple rules.

- 1) If DIFFERENCE is greater than a prescribed threshold, the threshold check reduces the value of SURF; the float will surface more frequently and obtain more localization fixes with GPS.
- 2) If DIFFERENCE is less than a prescribed threshold, the threshold check makes the value of SURF larger; the float will surface less often. This feature prevents a high frequency of surfacings, e.g., every hour.

The parameter SURF is bounded both above and below, hence we avoid the following: 1) the float surfaces every hour to obtain a new prediction; and 2) the float never surfaces to update the ROMS. This is implemented via a saturation function augmented into the closed-loop system in Fig. 6.

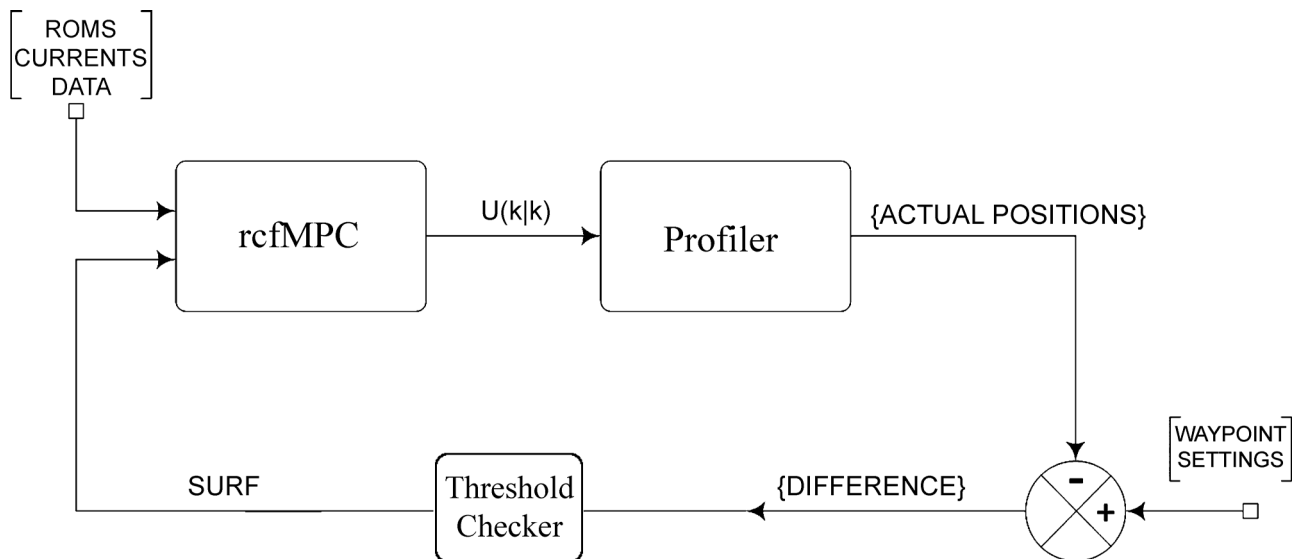


Fig. 6. Feedback of the surfacing signal (SURF) to form a closed-loop system.

## IX. SIMULATION RESULTS

We present three results of the application of the proposed RCFMPC in a simulated scenario to steer a profiling float between two given waypoints. For each example, we set the radius  $r$  of the ball  $\mathcal{B}_r$  to 350 m. This choice of  $r$  was motivated by the analysis of vehicle navigation in the deployment region presented in [26] and [27], and iteratively updated through multiple simulation trials. As shown in Section VIII-A, the selection of  $r$  depends on the form of the matrix  $\mathbf{B}$ ; the ocean model predictions. This directly correlates to the magnitude of the ambient currents, distance between waypoints along the prescribed path, and resolution of the underlying ocean model. Additionally, the size of  $r$  will depend on the trust in the model predictions, since even if the optimal  $r$  is chosen based on the aforementioned parameters, it is only optimal if the prediction matches reality. A detailed analysis on the choice of  $r$  is out of scope of this presentation, but is the subject of ongoing research.

### A. Scenario 1: Initial Test

As an initial trial case, we considered 16 days of ROMS predictions from July 2011. These data were used to compute the controllability map and plan the path presented in Fig. 5. We consider controlling the float between START and WP1 of this computed path to initially demonstrate the proposed controller and methodology.

The plot in Fig. 7 shows the computed control for the float as the prescribed depth with respect to time. Given the ocean currents described earlier, it takes the float 52 h to navigate from the start location to WP1 in the computed path shown in Fig. 5. Note that there were multiple instances when the currents on the sea surface were in the direction of the goal. Thus, for an actual deployment, we would have been able to update the position information frequently; approximately every 10 h. In the time epoch before rising to the sea surface, the vehicle descends to the seabed, ensuring the float will travel through the whole water column. This behavior is observed at  $t = 10, 18, 27, 35,$  and  $45$  h.

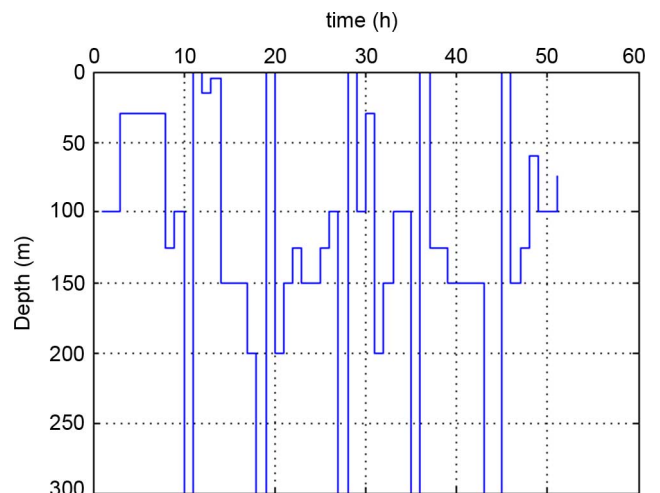


Fig. 7. A plot of the prescribed depth of the float versus time as computed by the RCFMPC.

For the prescribed depths shown in Fig. 7, the simulated path executed by the vehicle is given by the red (dashed) line in Fig. 8. Note that this path is projected up to the sea surface. The starting location is marked by a green circle, and the desired goal is given by a red star. The solid blue line denotes the straight line path connecting the two waypoints. The final destination achieved by the vehicle is denoted by the black square at the end of the dashed path. The terminal location of the float is within the 350-m radius around the waypoint. We remark that the final destination of the float and the goal location will rarely coincide due to the parameter  $r$  and the speed of the ocean currents. Once the float is inside  $\mathcal{B}_r$ , the waypoint is considered achieved. For this validation scenario, it is evident from Fig. 8 that a profiling float is capable of utilizing ocean currents to achieve a path that was computed by maximizing predicted controllability.

As a comparison to the controlled path presented in Fig. 8, we provide an example of uncontrolled drifting motion in Fig. 9. We present three scenarios of prescribing a constant depth for the float: ocean surface (0 m), 50-m depth, and 100-m depth. Additionally, we present the motion of a float that executes a preset

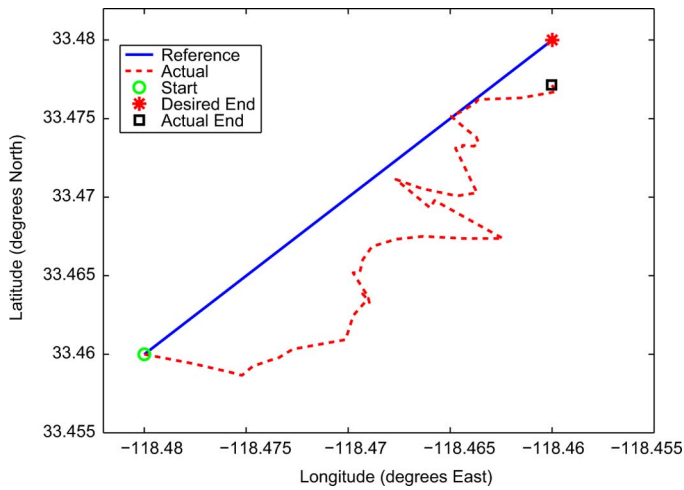


Fig. 8. The path followed by the profiling float (red, dashed line) by executing the control presented in Fig. 7. The straight line path between waypoints is given by the blue (solid) line.

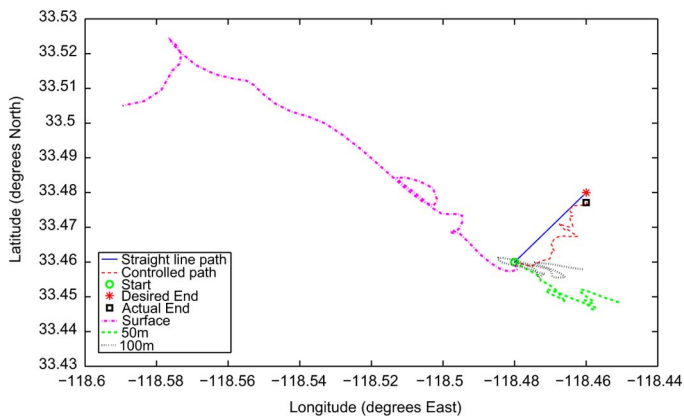


Fig. 9. The path followed by the profiling float following our proposed control (red, dashed line), remaining only at the sea surface (magenta, dashed-dotted line), a constant depth of 50 m (green, dashed line), and a constant depth of 100 m (black, dotted line). The solid blue line is the straight line path connecting the two waypoints.

profile mission similar to the standard Argo mission shown in Fig. 3. This preset profile starts at the surface for 1 h, dives to 100 m, and remains there for 6 h, then returns to the surface for 1 h to repeat the entire process.

Here, we see that a constant depth selection, and a fixed mission profile based on a standard profiling pattern both lead to rapid divergence of the float from the prescribed path. In the case of restriction to utilizing only surface currents, the float diverges away from the region of interest. Since the mission restricted to the surface extremely deviated from the prescribed area, a magnified view of Fig. 9 is given in Fig. 10 to better compare the results.

### B. Scenario 2: Float Control During the Upwelling Season

Given the initial results of scenario 1 presented in Section IX-A, we now examine the application of persistent monitoring with a profiling float off the coast of southern California. Specifically, we aim to investigate whether it is feasible for a profiling float to continually traverse the channel. First, we consider controlling the float during the March–June timeframe (the upwelling season). The first 24 h of each ROMS prediction from March 1, 2010 through June 30, 2010 were merged to create a

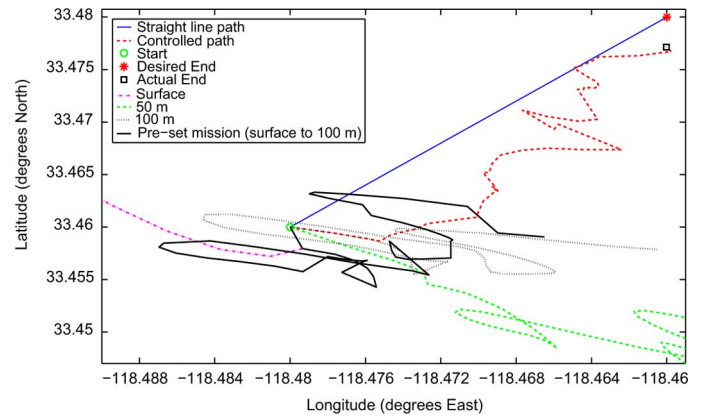


Fig. 10. A magnified view of Fig. 9, including the path for the preset standard profile (solid black line).

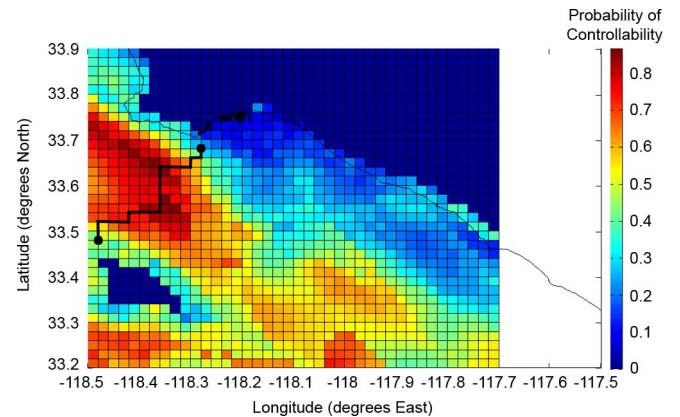


Fig. 11. Controllability map and the planned path (black line) for a profiling float to traverse the SPB channel during the 2010 upwelling season (March 1 through June 30).

virtual ocean current simulation of duration 2928 h. We computed the controllability map shown in Fig. 11 using the first 500 h of these data. The remaining  $\sim 2400$  h of the data were used to provide model updates as the float progressed through the mission. The computed controllability map was used as the input scalar field to the A\* path planner, along with start and end locations on either side of the channel. In Fig. 11, we display the path computed by the A\* planner, which denotes the path of highest percentage of controllability for a profiling float. We simulated the execution of this path from the start to the goal waypoint, and then back to the original start location. The computed depths to follow the prescribed path are presented in Fig. 12. Following this depth profile through the ocean model data, the path that was followed by the float (projected to the ocean surface) is presented in Fig. 13. The initial traversal took just longer than 600 h, while the return trip to the starting location took the float almost 1000 h.

### C. Scenario 3: Float Control During the Summer/Early Fall Season

We consider controlling the float during the June–October timeframe (the summer/early fall season). The first 24 h of each ROMS prediction from June 1, 2010 through October 31, 2010 were merged to create a virtual ocean current simulation of duration 3672 h. Note that since the data for the upwelling season and the summer/early fall seasons overlap, we can merge the



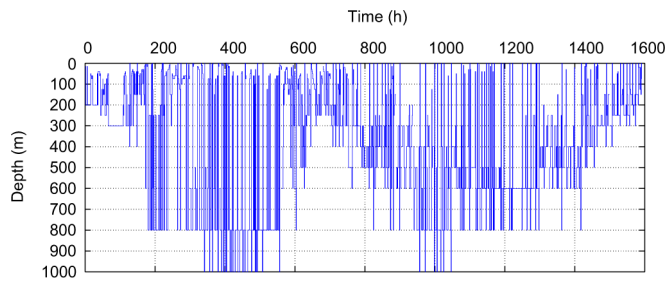


Fig. 12. A plot of the prescribed depth of the profiling float versus time to traverse the SPB channel during the 2010 upwelling season, as computed by the RCFMPC.

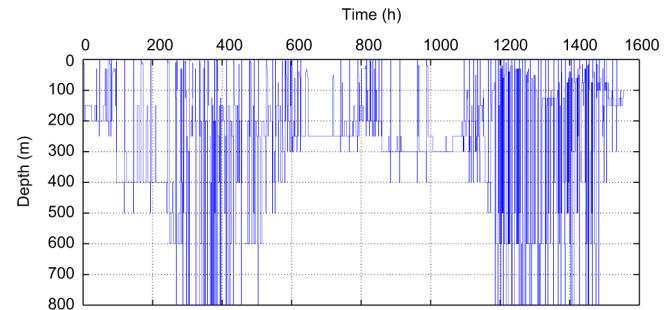


Fig. 15. A plot of the prescribed depth of the profiling float versus time to traverse the SPB channel during the 2010 summer/early fall season, as computed by the RCFMPC.

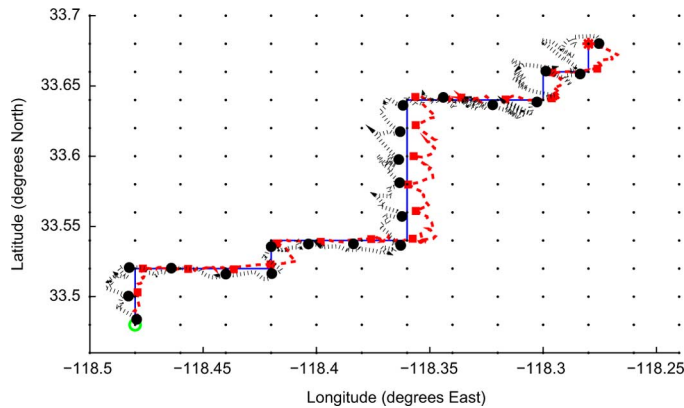


Fig. 13. The path followed by the profiling float from the start to the goal (dashed red line), and from the goal back to the start (dotted black line) by executing the control presented in Fig. 12. The solid blue line marks the prescribed optimal controllability path computed by the A\* planner. The black circles and red squares represent the location of the float when it achieved each prescribed waypoint, with the dashed lines indicating the path traversed by the float. The black dots denote the location of the nodes of the ROMS grid.

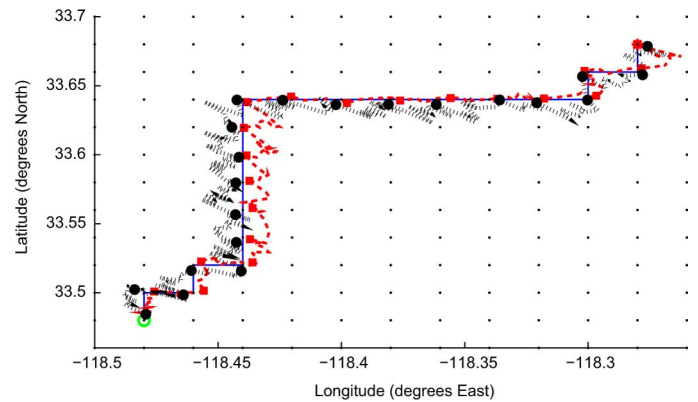


Fig. 16. The path followed by the profiling float (dashed red line) from the start to the goal, and from the goal back to the start (dotted black line) by executing the control presented in Fig. 15. The solid blue line marks the prescribed optimal controllability path computed by the A\* planner. The black circles and red squares represent the location of the float when it achieved each prescribed waypoint, with the dashed lines indicating the path traversed by the float. The black dots denote the location of the nodes of the ROMS grid.

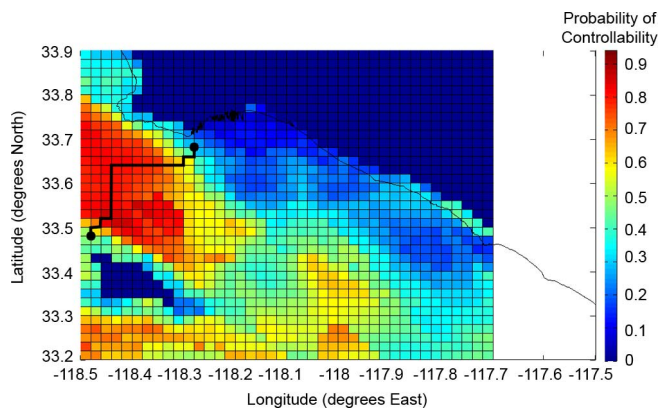


Fig. 14. Controllability map and the planned path (black line) for a profiling float to traverse the SPB channel during the summer/early fall season (June 1, 2010 through October 31, 2010).

results of this section with the previous results to demonstrate continuous control across two seasons. Based on the first 500 h of these data, we computed the controllability map shown in Fig. 14. The computed controllability map and the path of highest percentage of controllability are displayed in Fig. 14. We simulated the execution of this path from the start to the goal waypoint, and then back to the original start location. The computed depths to follow the prescribed path are presented in Fig. 15. Following this depth profile through the ocean model

data, the path that was followed by the float (projected to the ocean surface) is presented in Fig. 16.

For this season, we see more symmetrical traversal times, with each taking approximately 800 h.

#### D. Restriction to Shallow Water

The motivation of this work focused on a cost-effective platform to perform persistent monitoring. In underwater applications, such a platform would be restricted to shallow waters, i.e.,  $<300$  m. In Sections IX-A–IX-C, we demonstrated the control of a profiling float by utilizing the entire water column through the channel, including depths up to 1000 m. Designing a vehicle, even a simple profiling float, for these depths would incur significant expenses due mainly to the pressure experienced. Hence, we reexamine the scenario presented in Sections IX-B and IX-C with a restriction to the upper 300 m of the water column through the channel.

Water velocity decreases with depth (see Fig. 4). Below  $\sim 200$  m, the velocity is near zero, and remains relatively constant throughout the remainder of the water column for most of the area of interest. Given these assumptions, we utilize the same controllability maps and the same paths as previously presented. In Fig. 17, we present the execution of the path from Section IX-B with a restriction to the upper 200 m of the water column. Fig. 18 presents the execution of the path from

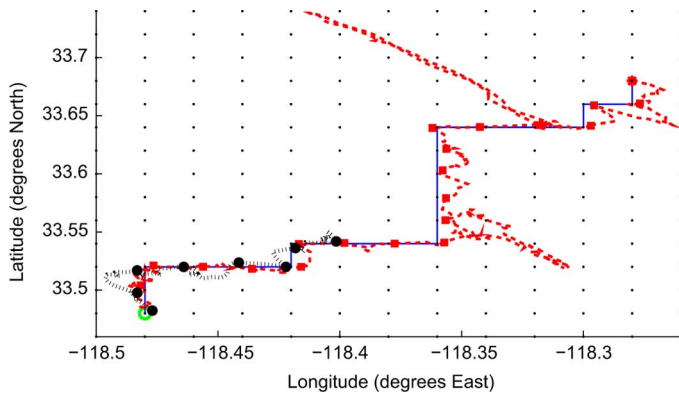


Fig. 17. The path followed by the profiling float from the start to the goal (dashed red line), and from the goal back to the start (dotted black line) for the upwelling season when restricted to the upper 200 m of the water column. The path computed by the A\* planner is given by the solid blue line. The black dots denote the location of the nodes of the ROMS grid.

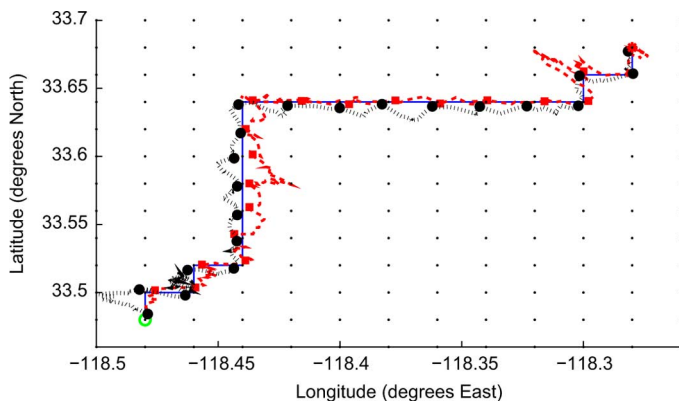


Fig. 18. The path followed by the profiling float from the start to the goal (dashed red line), and from the goal back to the start (dotted black line) for the summer/early fall season when restricted to the upper 300 m of the water column. The path computed by the A\* planner is given by the solid blue line. The black dots denote the location of the nodes of the ROMS grid.

Section IX-C with a restriction to the upper 300 m of the water column.

We notice two large deviations from the prescribed one in Fig. 17 and one deviation in Fig. 18 that did not occur in Figs. 13 and 16, respectively. These deviations are a result of the float not being able to descend all the way to the seafloor to experience near-zero currents while awaiting more favorable currents in the water column above. Although we make the assumption that currents below  $\sim 200$  m are near zero, they are not identically zero and have some effect on the drifting vehicle. In the two cases presented, although the ocean currents were small, the portion of the water column utilized for the control did not have adequate variability in direction to provide sufficient controllability. These deviations can be minimized by computing a separate controllability map and path plan that are depth restricted. For the study here, we are interested in feasibility of the proposed method, which was demonstrated through the previous discussions. Future field trials will further investigate the implementability of the proposed methods and controller.

## X. CONCLUSION

To start this paper, we posed the question: “Can you control the horizontal motion of a profiling float?” The simulations and

analyses presented lead us to answer: “Probably.” The factors to consider that do not allow us to answer this question as outright affirmative are the resolution and accuracy of the model predictions, and the desired accuracy of the specific application or experiment. However, it is clear that a broad level of controllability is achievable by the system considered.

Here, we have provided the basic details of profiling or Lagrangian floats, along with a derivation of reformulated equations of motion for the considered application. We utilize these equations to present an analysis of controllability by considering ocean currents as input controls rather than disturbances. From this perspective, we then demonstrate how ocean model predictions are used to create controllability maps for large ocean regions. Path planning is done with a standard A\* planner, computing a path that provides the highest probability of controllability between start and goal locations.

We motivate the analyses with science-driven questions that require additional constraints on the controller design. Given the start and goal locations, and the ocean current predictions, we implement an RCFMPC to compute the depth control to implement for the float to navigate between the prescribed locations. This study utilized historical model data that were implemented in the simulation environment as if the model were producing outputs in real time. Specifically, we did not provide the controller more than 72 h of predictions at any one time step in the simulation execution. For this reason, we imposed the constraint of surfacing at least every 70 h, and remaining on the surface for at least 1 h at each surfacing. These constraints ensure an accurate prediction and allow ample time for data to be transferred and new depth controls to be computed.

The control theory presented in Sections V and VI merged with the controller described in Section VIII is validated through the simulation results presented in Section IX. In these results, we show three scenarios in which simply controlling the operational depth of a float guarantees broad controllability results, such as navigating from one location to another. Additionally, we demonstrate that the full water column is not needed for implementing this approach, as the upper water column in the selected region has enough current variability to provide controllability to a profiling float. The presented simulations are for a mission off the coast of Los Angeles, and they show encouraging results in the ability of a drifting vehicle to maintain a prescribed course and reach a desired location. This same method can also be implemented to keep a profiling float within a certain region for an extended period of time; exploitations of ocean currents that do not move it away from a desired location. These results motivate field trials to further validate the control theory and path-planning methods presented in this study.

The results presented here hold as long as we allow the float to move vertically through the water column uninhibited; this is not actually the case. Thus, a model for the vertical motion of a float needs to be incorporated into the theory to provide a more precise prediction on the locations of controllability, as well as how the control is executed for estimating the path-following ability of the vehicle. Coupling this with a temporal analysis of the variability of the percentage of the region where a float can be controlled will provide valuable information for preparing for field deployments.

The simulation results presented in Sections IX-A–IX-C provide ample motivation for performing field trials. For deployment of floats within shallow, coastal zones, there will be a compromise between endurance and depth cycling capability. To this end, a profiling float is currently under development for validating the results of this research. The aim is to design a vehicle that can exploit the controllability results presented here by moving vertically through the water column, and which has the ability to remain on deployment for  $>3$  months. We remark that the limiting factor for increasing the deployment life of a profiling float is the changes in buoyancy. Computational requirements for the implementation of the methods proposed here are minimal. The controllability map and the prescribed path would be computed before deployment. This is primarily due to the large amount of data upon which the computations are based. Given the data, computation of the controllability map and A\* path takes approximately 2 min on a 2.66-GHz processor with 8-GB RAM. The control actions would be computed onboard with each update to the model predictions (upon surfacing). Computing the three months of control actions, as presented in Figs. 12 and 15, requires approximately 5 min on a 2.66-GHz processor with 8-GB RAM. Given that the transfer of new model data for this computation will take less than 10 min and that float will stay on the surface for 1 h, this is ample time for updating the prescribed depths for the upcoming segments.

## REFERENCES

- [1] M. Belbeoch, "Argo—Part of the integrated global observation strategy," Dec. 2012 [Online]. Available: <http://www.argo.ucsd.edu/index.html>, 2010
- [2] K. A. Morgansen, B. I. Triplett, and D. J. Klein, "Geometric methods for modeling and control of free-swimming fin-actuated underwater vehicles," *IEEE Trans. Robot.*, vol. 23, no. 6, pp. 1184–1199, Dec. 2007.
- [3] J. Manley and S. Wilcox, "The wave glider, a persistent platform for ocean science," in *Proc. MTS/IEEE OCEANS Conf.*, Sydney, Australia, May 2010, DOI: 10.1109/OCEANSSYD.2010.5603614.
- [4] Webb Research Corporation, "Slocum glider," Mar. 2011 [Online]. Available: <http://www.webbresearch.com/slocum.htm>, 2008
- [5] Hydroid, LLC, "Remus 600," May 2008 [Online]. Available: <http://www.hydroidinc.com/remus600.html>, 2008
- [6] O. Schofield, J. Kohut, D. Aragon, E. Creed, J. Graver, C. Haldman, J. Kerfoot, H. Roarty, C. Jones, D. Webb, and S. Glenn, "Slocum gliders: Robust and ready," *J. Field Robot.*, vol. 24, no. 6, pp. 473–485, 2007.
- [7] G. Griffiths, C. Jones, J. Ferguson, and N. Bose, "Undersea gliders," *J. Ocean Technol.*, vol. 2, no. 2, pp. 64–75, 2007.
- [8] D. Roemmich, S. Riser, R. Davis, and Y. Desaubies, "Autonomous profiling floats: Workhorse for broad-scale ocean observations," *Mar. Technol. Soc. J.* vol. 38, pp. 21–29, 2004.
- [9] C. Roman, G. Inglis, and B. McGilvray, "Lagrangian floats as sea floor imaging platforms," *Continental Shelf Res.* vol. 31, no. 15, pp. 1592–1598, 2011.
- [10] J. G. Graver, "Underwater gliders: Dynamics, control and design," Ph.D. dissertation, Dept. Mech. Aerosp. Eng., Princeton Univ., Princeton, NJ, USA, 2005.
- [11] D. Paley, F. Zhang, and N. Leonard, "Cooperative control for ocean sampling: The glider coordinated control system," *IEEE Trans. Control Syst. Technol.* vol. 16, no. 4, pp. 735–744, Jul. 2008.
- [12] N. E. Leonard, D. A. Paley, R. E. Davis, D. M. Fratantoni, F. Lekien, and F. Zhang, "Coordinated control of an underwater glider fleet in an adaptive ocean sampling field experiment in Monterey Bay," *J. Field Robot.* vol. 27, no. 6, pp. 718–740, 2010.
- [13] C. Petres, Y. Pailhas, P. Patron, Y. Petitot, J. Evans, and D. Lane, "Path planning for autonomous underwater vehicles," *IEEE Trans. Robot.*, vol. 23, no. 2, pp. 331–341, Apr. 2007.
- [14] A. Alvarez, A. Caiti, and R. Onken, "Evolutionary path planning for autonomous underwater vehicles in a variable ocean," *IEEE J. Ocean. Eng.*, vol. 29, no. 2, pp. 418–429, Apr. 2004.
- [15] B. Garau, A. Alvarez, and G. Oliver, "Path planning of autonomous underwater vehicles in current fields with complex spatial variability: An A\* approach," in *Proc. IEEE Int. Conf. Robot. Autom.*, Barcelona, Spain, 2005, pp. 194–198.
- [16] D. Kruger, R. Stolkin, A. Blum, and J. Briganti, "Optimal AUV path planning for extended missions in complex, fast-flowing estuarine environments," in *Proc. IEEE Int. Conf. Robot. Autom.*, Rome, Italy, 2007, pp. 4265–4270.
- [17] J. Witt, M. Dunbabin, J. Kim, and R. Mahony, "Go with the flow: Optimal path planning in coastal environments," in *Proc. Australasian Conf. Robot. Autom.*, 2008, pp. 1–9, ISBN: 9780646506432.
- [18] M. T. Wolf, L. Blackmore, Y. Kuwata, N. Fathpour, A. Elfes, and C. Newman, "Probabilistic motion planning of balloons in strong, uncertain wind fields," in *Proc. IEEE Int. Conf. Robot. Autom.*, Anchorage, AK, USA, May 2010, pp. 1123–1129.
- [19] K. Szwajkowska and F. Zhang, "A lower bound on navigation error for marine robots guided by ocean circulation models," in *Proc. IEEE/RSJ Int. Conf. Intell. Robot. Syst.*, San Francisco, CA, USA, 2011, pp. 3583–3588.
- [20] K. P. Dahl, D. R. Thompson, D. McLaren, Y. Chao, and S. Chien, "Current-sensitive path planning for an underactuated free-floating ocean sensorweb," in *Proc. IEEE/RSJ Int. Conf. Intell. Robot. Syst.*, San Francisco, CA, USA, Sep. 2011, pp. 3140–3146.
- [21] Center for Ocean-Atmospheric Prediction Studies (COAPS), "Hybrid coordinate ocean model (hycom)," Jan. 2013 [Online]. Available: <http://hycom.org/dataserver/glb-analysis/expt-90pt8>,
- [22] J. Jouffroy, Q. Zhou, and O. Zielinski, "Towards selective tidal-stream transport for Lagrangian profilers," in *Proc. MTS/IEEE OCEANS Conf.*, Kona, HI, USA, Sep. 2011.
- [23] J. Jouffroy, Q.-Y. Zhou, and O. Zielinski, "On active current selection for Lagrangian profilers," *Model. Identif. Control*, vol. 34, no. 1, pp. 1–10, 2013, DOI: 10.4173/mic.2013.1.1.
- [24] R. N. Smith and M. Dunbabin, "Controlled drift: An investigation into the controllability of underwater vehicles with minimal actuation," in *Proc. Australasian Conf. Robot. Autom.*, Jul. 2011, EP115751.
- [25] R. N. Smith and V. T. Huynh, "Controlling minimally-actuated vehicles for applications in ocean observation," in *Proc. IFAC Workshop Navigat. Guid. Control Underwater Veh.*, Porto, Portugal, Apr. 2012, pp. 1–8.
- [26] R. N. Smith, J. Kelly, Y. Chao, B. H. Jones, and G. S. Sukhatme, "Towards improvement of autonomous glider navigation accuracy through the use of regional ocean models," in *Proc. 29th Int. Conf. Offshore Mech. Arctic Eng.*, Shanghai, China, Jun. 2010, pp. 597–606.
- [27] R. N. Smith, J. Kelly, and G. S. Sukhatme, "Towards improving mission execution for autonomous gliders with an ocean model and Kalman filter," in *Proc. IEEE Int. Conf. Robot. Autom.*, Minneapolis, MN, USA, May 2012, pp. 4870–4877.
- [28] H. Rosaby, E. Levine, and D. Connors, "The isopycnal swallow float—a simple device for tracking water parcels in the ocean," *Progr. Oceanogr.*, vol. 14, pp. 511–525 [Online]. Available: <http://www.sciencedirect.com/science/article/B6V7B-48CFVX9-3C/2/a75ce27>
- [29] R. E. Davis, "Observing the general circulation with floats," *Deep Sea Res.*, vol. 38, no. Suppl. 1, pp. 531–571, 1991.
- [30] R. E. Davis, D. Webb, L. Regier, and J. Dufour, "The autonomous Lagrangian circulation explorer (alace)," *J. Atmos. Ocean. Technol.*, vol. 9, pp. 264–285, 1992.
- [31] E. A. D'Asaro, D. M. Farmer, J. T. Osse, and G. T. Dairiki, "A Lagrangian float," *J. Atmos. Ocean. Technol.*, vol. 13, pp. 1230–1246, 1996.
- [32] Q. Vu, "SOLO-TREC: Sounding oceanographic Lagrangian observer (SOLO) thermal recharging (TREC)," Dec. 2012 [Online]. Available: <http://solo-trec.jpl.nasa.gov/SOLO-TREC/2012>
- [33] A. Shchepetkin and J. McWilliams, "Quasi-monotone advection schemes based on explicit locally adaptive dissipation," *Monthly Weather Rev.*, vol. 126, pp. 1541–1580, 1998.
- [34] A. F. Shchepetkin and J. C. McWilliams, "The regional oceanic modeling system (ROMS): A split-explicit, free-surface, topography-following-coordinate oceanic model," *Ocean Model.*, vol. 9, pp. 347–404, 2005.
- [35] R. N. Smith, Y. Chao, P. P. Li, D. A. Caron, B. H. Jones, and G. S. Sukhatme, "Planning and implementing trajectories for autonomous underwater vehicles to track evolving ocean processes based on predictions from a regional ocean model," *Int. J. Robot. Res.*, vol. 29, no. 12, pp. 1475–1497, Oct. 2010.
- [36] R. N. Smith, M. Schwager, S. L. Smith, B. H. Jones, D. Rus, and G. S. Sukhatme, "Persistent ocean monitoring with underwater gliders: Adapting sampling resolution," *J. Field Robot.*, vol. 28, no. 5, pp. 714–741, Sep./Oct. 2011.

- [37] W.-L. Chow, "Über systemen von linearen partiellen differentialgleichungenerster ordnung," *Mathematische Annalen*, vol. 117, pp. 98–105, 1939.
- [38] H. Sussmann and V. Jurdjevic, "Controllability of nonlinear systems," *J. Diff. Equations*, vol. 12, pp. 95–116, 1972.
- [39] F. Bullo and A. D. Lewis, *Geometric Control of Mechanical Systems*. New York, NY, USA: Springer-Verlag, 2005, ch. 3–6.
- [40] R. Bianchini and G. Stefani, "Controllability along a trajectory: A variational approach," *SIAM J. Control Optim.*, vol. 31, no. 4, pp. 900–927, 1993.
- [41] M. Noble, B. Jones, P. Hamilton, J. Xu, G. Robertson, L. Rosenfeld, and J. Largier, "Cross-shelf transport into nearshore waters due to shoaling internal tides in San Pedro Bay, CA," *Continental Shelf Res.*, vol. 29, no. 5, pp. 1821–1835, 2009.
- [42] P. Hamilton, M. A. Noble, J. Largier, L. K. Rosenfeld, and G. Robertson, "Cross-shelf subtidal variability in San Pedro Bay during summer," *Continental Shelf Res.*, vol. 26, no. 6, pp. 681–702, 2006.
- [43] M. Kvasnica, P. Grieder, and M. Baotic, "Multi-parametric toolbox (MPT)," 2004 [Online]. Available: <http://control.ee.ethz.ch/mpt/>
- [44] J. Löfberg, "Yalmip: A toolbox for modeling and optimization in MATLAB," in *Proc. IEEE Int. Symp. Comput.-Aided Control Syst. Design Conf.*, Taipei, Taiwan, 2004, pp. 284–289.
- [45] J. Acevedo and E. N. Pistikopoulos, "A multiparametric programming approach for linear process engineering problems under uncertainty," *Ind. Eng. Chem. Res.*, vol. 36, no. 3, pp. 717–728, 1997.
- [46] V. Dua and E. N. Pistikopoulos, "An algorithm for the solution of multiparametric mixed integer linear programming problems," *Ann. Oper. Res.*, vol. 99, pp. 123–139, Dec. 2000 [Online]. Available: <http://dx.doi.org/10.1023/A:1019241000636>
- [47] A. Bemporad, F. Borrelli, and M. Morari, "Optimal controllers for hybrid systems: Stability and piecewise linear explicit form," in *Proc. IEEE Conf. Decision Control*, Sydney, Australia, Dec. 2000, vol. 2, pp. 1810–1815.



**Ryan N. Smith** (M'10) received the B.S. degrees in both mathematics and engineering physics from Miami University, Oxford, OH, USA, in 1998 and the M.A. degree in mathematics and the Ph.D. degree in ocean & resources engineering from the University of Hawaii at Manoa, Honolulu, HI, USA, in 2002 and 2008, respectively.

He was a Postdoctoral Research Associate in the Robotics Embedded Systems Laboratory, University of Southern California, Los Angeles, CA, USA, during 2009–2010, and a Lecturer in the School of Electrical Engineering and Computer Science, Queensland University of Technology, Brisbane, Qld., Australia, in 2011–2013. He is currently an Assistant Professor in the Engineering and Physics Department, Fort Lewis College, Durango, CO, USA.



**Van T. Huynh** (S'11) received the B.E. degree in mechatronics from the Ho Chi Minh City (HCMC) University of Technology, Vietnam National University, Ho Chi Minh City, Vietnam, in 2006 and the M.E. degree in automatic control engineering from the University of New South Wales, Sydney, N.S.W., Australia, in 2011. Currently, he is working toward the Ph.D. degree in robotics at the School of Electrical Engineering and Computer Science, Queensland University of Technology, Brisbane, Qld., Australia.

His research interests include nonlinear robust and adaptive control, optimization in path planning and control, Bayesian inference in robotics, and science-driven applications for autonomous underwater vehicles.